Geothermics 55 (2015) 58–68

Contents lists available at ScienceDirect

Geothermics

journal homepage: www.elsevier.com/locate/geothermics

Integrated assessment of variable density–viscosity groundwater flow for a high temperature mono-well aquifer thermal energy storage (HT-ATES) system in a geothermal reservoir

Răzvan Mihai Zeghici[a,*], Gualbert H.P. Oude Essink[b,e], Niels Hartog[c,e,1], Wijbrand Sommer[b,d,2]

[a] Faculty of Building Services, RO, Romania
[b] DELTARES, Unit of Subsurface and Groundwater Systems, Utrecht, NL, Netherlands
[c] KWR Watercycle Research Institute, NL, Netherlands
[d] Wageningen University, NL, Netherlands
[e] Utrecht University, Faculty of Geosciences, Utrecht, NL, Netherlands

ARTICLE INFO

Article history:
Received 18 May 2013
Accepted 31 December 2014

Keywords:
High temperature aquifer thermal energy storage (HT-ATES)
Porous media
Groundwater
Variable density and viscosity
Dispersivity analyses
Case-study in Bucharest

ABSTRACT

The use of groundwater systems for heat storage increasingly gains interest among water managers, policy makers and researchers as a way to increase the efficiency of energy production and to allow the re-use of waste heat. Typically, mono-well storage systems are thought to require the use of separate aquifers. This study assessed the suitability of using heat and cold storage in a single deep geothermal aquifer for district heating and cooling. An integrated modelling approach was used for evaluating the controls on the energy efficiency of high temperature aquifer thermal energy storage (HT-ATES). The temperature difference (ΔT) of 40 °C between the injection temperatures for the cold and warm storages 20 °C and 60 °C was significant, which required accounting for transient variation of density and viscosity due to temperature and pressure within the modelling code SEAWAT. The developed model was applied for a geothermal reservoir from the Moesian platform, in the Bucharest area, Romania. The sensitivity of the system efficiency was analyzed with respect to the main physical (density, viscosity, longitudinal dispersivity) and operational design parameters (distance between warm and cold storage volumes, flow rates). Uncertainties in geological heterogeneity and the associated range in longitudinal dispersivity values (5–50 m) resulted in significant efficiency differences (80–55%). While reducing the lateral distance between multiple mono-well systems increased their overall efficiency due to positive thermal interference, a minimum vertical distance of (160 m) was required between the injection/extraction filters to prevent interaction between the cold and warm storage volumes. Overall, this study highlights the potential of using a cost-effective mono-well system for HT-ATES in single deep geothermal groundwater systems.

1. Introduction

During the past decade, a rising demand for sustainable energy sources and CO_2 emission reduction has led to intensified use of aquifer thermal energy storage (ATES) systems, a cost-effective energy technology in support of ambitions for CO_2 emission reductions. This technology provides seasonal heating and cooling for buildings by means of the alternating injection and extraction of heated (injection during summer, extraction during winter) and cooled (injection during winter, extraction during summer) groundwater via wells in aquifers (Molz et al., 1978, 1979, 1981, 1983; Tsang et al.,1980; Edworthy and Puri, 1986; Carotenuto et al., 1991; Kim et al., 2010).

Most of these ATES systems are operated with limited temperature differences ($\Delta T < 15$ °C) between warm (<20 °C) and cold wells (>5 °C) in shallow aquifers (down to 200 m) with an ambient groundwater temperature of ~11 °C. An increasing number of ATES systems are reported in Europe and elsewhere (Gao et al.,

* Corresponding author. Tel.: +40 728 123 887.
E-mail addresses: razvan.zeghici@gmail.com (R.M. Zeghici), gualbert.oudeessink@deltares.nl (G.H.P. Oude Essink), niels.hartog@kwrwater.nl (N. Hartog), wijbsommer@hotmail.com (W. Sommer).
[1] Tel.: +31 306069652.
[2] Tel.: +31 317483339.

http://dx.doi.org/10.1016/j.geothermics.2014.12.006
0375-6505/

2009; Sanner et al., 2003). While the number of ATES systems that operate at higher temperatures is still relatively limited, the use of high temperature aquifer thermal energy storage systems (HT-ATES) provides the advantage of higher temperature differences (ΔT's) which increases both the overall energy storage capacity and energy efficiency (Drijver et al., 2012; Kabus et al., 2009). Particularly, the implementation of HT-ATES has potential in combination with district heating as well as cooling applications, as high temperature storage provides important flexibility to interconnect multiple energy sources (such as gas fired cogeneration turbines, solar collectors, waste heat, water source heat pumps). Since high temperature storage is typically performed at much greater depths than conventional ATES systems, significant investment costs are associated with well drilling. While the use of a mono-well system, in which cold and warm storage is separated vertically rather than horizontally, could considerably reduce the investment costs for such systems, increases the risk of negative impact on thermal efficiency due to interaction between hot and cold storage volumes. Therefore, vertical separation of heat and cold storage by an aquitard is typically considered for HT-ATES systems.

This study required simulation of various configurations for the use of mono-well HT-ATES systems within a single aquifer, using favourable storage temperatures not only for district heating but also for district cooling. For classical cooling solutions it is common to use chilled water below 10 °C but new cooling concepts use cooling sources even over 20 °C; especially in temperate continental countries where the average temperature in summer exceeds 30 °C and the peaks are above 40 °C. Façade cooling or asphalt cooling can also be considered as district cooling applications for which 20 °C brackish water may be a proper source (Zeghici et al., 2014).

The main objective of this study was to assess the sensitivity of the main parameters that affect HT-ATES efficiency, including density and viscosity variations, through numerical modelling using the SEAWAT code, for water mass and heat transport.

2. Theoretical background

The main operational aspect related to ATES systems is the amount of the thermal energy which can be recovered after a previous injection, which is expressed as the "Energy efficiency" (E) [%]. Energy efficiency is calculated as the ratio between discharged energy recovered and the initially recharged energy, following an injection and extraction cycle:

$$E = \frac{E_{extraction}}{E_{injection}}[\%] \quad (1)$$

where $E_{injection}$ [MWh/yr] is the recharged energy (injected in the storage) and $E_{extraction}$ [MWh/yr] is the discharged energy (extracted from storage). Thermal energy is calculated for the time t, using the temperature of the injected water $T(t)$ which is the temperature in the well, in reference to T_0 which is the temperature of the undisturbed aquifer.

In shallow applications, an energy balance is achieved when the average temperature difference ΔT between the cold storage and warm storage is centred at the environmental background temperature of the aquifer and applying the same seasonal flow rate in cooling and heating mode. An energy balance is important for a sustainable operation of the ATES systems that is required to deliver both cooling and heating capacities. For example, when more heat is injected into the aquifer during summer, than extracted during winter, this may lead to a gradual warming of the aquifer, making it less suitable for cooling purposes.

The subsurface is characterized by a variable spatial distribution of lithological layers with various hydraulic conductivities, resulting in various degrees of physical heterogeneity that affect water transport. Recent studies show that energy efficiency (E) of ATES systems is generally lower for heterogeneous aquifers than for homogeneous aquifers (Chaudhuri and Sekhar, 2006, Ferguson, 2007; Sommer et al., 2013). This is due to the wider spread of the thermal storage volume in heterogeneous which increases mixing surfaces with the environment. The associated energy loss can be related to the macro-dispersion coefficient which describes groundwater flow due to local variations in the velocity caused by spatial heterogeneity (Nick et al., 2008).

Many laboratory studies and tracer measurements (Anderson, 2005; Vandenbohede and Lebbe, 2003, 2006; Vandenbohede et al., 2008, 2009) have illustrated the convection-conduction equation to provide a satisfactory description of the mixing process in groundwater applications. The Peclet number can be applied to assess the most dominant process. For small Peclet numbers (<1) the conductive fluxes (viz. the parabolic nature of the convection-conduction equation) prevails, whereas for large Peclet numbers (>2) the convective fluxes (the hyperbolic nature) dominate. For large *Peclet* numbers, the longitudinal dispersion coefficient increases linearly with injection velocity. At laboratory scales, longitudinal dispersivity, α_L is in the order of centimetres or decimetres but in the field it can range from one metre to tens of metres depending on formation heterogeneity (Marsily, 1986). It is certain that solute dispersivity increases with the application scale (Gelhar et al., 1992), as confirmed by the interpretation of different tracer tests (Vandenbohede and Lebbe, 2003, 2006; Vandenbohede et al., 2008). However, there is not a clear consensus on how best to represent the field-scale mixing process in a quantitative way (Gelhar et al., 1992).

Similarly, conflicting views on the importance of thermal dispersion can be found in literature. According to Marsily (1986), thermal dispersivity is analogous to solute dispersivity, having the same order of magnitude. However, other authors state assess the thermal dispersivity at one order of magnitude smaller (Smith and Chapman, 1983) or even neglect thermal dispersion for Peclet numbers smaller than 3000 (Bear, 1972; Hopmans et al., 2002).

A strong, physical, argument for dissimilarity states that heat is not only transported through pore water, but also through the sediment matrix and forms a more homogeneous medium (Vandenbohede et al., 2008). In this case, heat transport is caused in a large extent by thermal diffusivity, with the contribution of dispersion being significantly smaller. Therefore, the thermal exchange between the fluid and the porous matrix is an essential part of the heat transport in ATES systems and was considered in our SEAWAT modelling following the method of Thorne et al. (2006).

Relevant for the temperature-induced density differences in HT-ATES systems, experiments on longitudinal hydrodynamic dispersion reveal that less dense fluids are displaced by a denser fluid. Also raising the density difference between fluids will diminish the mixing (thermal loss) zone. Hassanizadeh (1990) and Hassanizadeh and Leijnse (1995) suggested a new nonlinear extension of Fick's law for high concentrations, confirmed by Schotting et al. in 1999. For a highly permeable porous medium, the density differences cause a decrease of the transverse dispersion. Also the mixing zone decreases for higher density differences (Grane and Gardner, 1961).

Overall, in a flow and transport regime there are two forms of convection: forced convection in which fluid motion is generated by an external source (e.g. hydraulic gradient) and free convection driven by density differences in the fluid occurring due to thermal gradients.

For storage in between two confining layers, a mixed convection regime is characterized as the ratio between theoretical free and forced velocities. According to Ward et al. (2007):

$$M = \frac{v_{free}}{v_{forced}} = \frac{2\pi rB}{Q}K\alpha \quad (2)$$

where r[m] is the plume radius, B[m] is the aquifer thickness, Q[m^3/day] is the pumping rate, K[m/day] is hydraulic conductivity and α[–] is the density difference ratio (aquifer water density/injected water density).

For $M \approx 1$, free and forced convection have the same order of magnitude. For $M \ll 1$ the system is dominated by forced convection (advection) and for $M \gg 1$, free convection is dominant.

For most of shallow ATES systems with limited temperature differences (<15 °C), free convection is much smaller than forced convection, and α can be neglected (Zuurbier et al., 2013). In HT-ATES applications (Kabus et al., 2009; Drijver, 2011; Bonte et al., 2012) where injection temperature in the warm well goes over 60 °C, density and viscosity differences becomes more significant. Therefore the mixed convection ratio is an important parameter for HT-ATES systems as the transition from a forced to a free convection dominated system results in a sharp lowering of efficiency (Ward et al., 2007). For $\alpha_L = 0.2$ m, system efficiency varies significantly for $0.1 < M < 1$ and for $\alpha_L > 10$ m, efficiency (E) is sensitive only when free convection is dominant. Free convection may become dominant for ATES systems in transition seasons, when water flow is limited, so if this occurs for extended periods a lower efficiency is expected.

The Richardson number, Ri represents a measure of the buoyancy effect relative to the inertia of the external forced or free stream flow on the heat and mass transfer. When $Ri \to 0$, forced convection is dominant in a mixed convection regime (Aydin and Kaya, 2009).

If the cold and warm plumes are situated above each other with no separation by strata of low permeability, as in the considered mono-well HT-ATES case, interference (shortage in the worst case) due to buoyancy effects might occur. The phenomena were studied using the correlation between buoyancy parameter (Richardson number) and local heat transfer coefficients where the Richardson number is written as:

$$R_i = \frac{g\beta(T_i - T_e)R_{th}^3}{\nu^2 Re^2} \tag{3}$$

where Reynolds number $Re = R_w U\rho/\mu$ is based on the injected water radius (R_w), average velocity (U), injected water density (ρ) and the dynamic viscosity (μ). The other components to calculate the Richardson number is also known as Grashof number formula which contains gravitational acceleration (g), thermal expansion coefficient (β), injection temperature (T_i) and environment temperature (T_e), thermal radius (R_{th}) and kinematic viscosity (ν).

For heat storage between two confining layers, the thermal radius is the radius that an injected cylindrically shaped thermal volume at constant temperature would have, with its thermal energy equal to the total heat energy of the injected fluid (Doughty et al., 1982). In our case, R_{th} is defined as:

$$R_{th} = \frac{V}{(\pi \cdot H)^{1/2}} \tag{4}$$

where V represents the thermal volume and H is the length of the well filter.

Within the thermal radius, heat transfer is governed by convection and dispersion. Outside the boundaries of the thermal radius, the process is dominated by conduction due to temperature gradients between injected liquid and undisturbed temperature of the environment. Mass transfer increases under favour of mixed convection and conduction. The larger values for conduction of heat arise partially because heat is transferred through the solid matrix as well as the fluid (Anderson, 2005). When two or several systems are placed too close to each other and boundaries interfere, their individual efficiency might be better or worse than without interference.

Studies on interactions between systems in one of the most ATES-dense regions in the Netherlands showed a general trend of increasing efficiency over time for wells placed at greater distance from each other and of lowering efficiency for systems which were located next to each other. However, in the ideal situation, such interactions between multiple ATES systems may help systems to trap energy within their capture zones leading to an increased efficiency of an individual ATES system (Bakr et al., 2013). If two or multiple water plumes of similar temperature are placed close enough to interact, their thermal gradient will decline towards zero over the interfered area, reducing conductive heat loss in the next cycles. On the other hand, if a cold plume is placed too close to one or multiple warm plumes, interference will generate a bigger thermal gradient, therefore increasing conductive heat loss.

3. Field case description

The field case for this HT-ATES study is situated in the Bucharest area in Romania (Fig. 1). Here, suitable water-saturated geological layers (either aquifers or geothermal basins) are typically found beneath 500 m below ground surface. Following the large scale geothermal gradient of about 25 °C per km (Fridleifsson et al., 2008), water temperature increases with depth but in specific areas, depending on hydro-geological structures, temperature distribution can vary strongly.

The HT-ATES model presented in this case study is positioned in a Dolomite-Carbonate Aquifer, with the lateral boundaries of the local model indicated in Fig. 1. The modelled area of interest is 64 km^2, sufficient to prevent any boundary effects on the thermal storage. The overall porosity in the formation, consisting of a matrix of fissures, is around 25%, indicating suitability for seasonal energy storage (Zeghici et al., 2013).

The geothermal aquifer is capped by an impermeable rock aquitard of which the bottom descends from −800 m in SSE to −1600 m in NNW. The pressure distribution confirms the regional groundwater flow (yellow arrow in Fig. 1) direction from SSE to NNW. The system is planned close to an existing, unexploited well, drilled in 1980s for underground exploration (Bandrabur et al., 1983; Bandrabur, 1988). The mono-well is placed in the centre of the discretized domain at approximately 4 km to the each surrounding boundary.

Fig. 2 illustrates the modelled well profiles for the first extraction cycles for the cold and warm storages used in the study case. The injection temperatures are 20 °C for the cold storage and 60 °C for the warm storage. The environment temperatures are 37.4 °C at the depth of the cold storage and 41.3 °C at the depth for the warm storage.

During injection, a part of the energy is dissipated as a result of mixing (heat conduction and interaction with solid matrix). Both components of injection (mixing and storage) are delimitated by the temperature profile in the wells (red and blue lines in Fig. 2).

The thickness of the aquifer is 1000 m on average which allows the cold and warm storages to be placed at different depths using a mono-well, although a suitable impermeable layer to separate these thermal storages seems to be lacking. Therefore, the cold storage filter was placed from −1500 to −1600 m and warm storage filter from −2010 to −2110 m (Fig. 4). Discharge is realized by submersible pumping from 120 m below surface (hydraulic head is set at 80 m below surface) (Bandrabur, 1988). The modelling parameters for the reference case are presented in Table 1.

In short, the mono-well used under these conditions for the new HT-ATES exploitation concept, consists of two hydraulically circuits, placed in one telescopic well (Fig. 3). The warm storage filter is formed of a metal liner. Above the liner there is metal fit out piece, protected by concrete casing. From here, the well is formed of prefabricated sections which host two hydraulic circuits, separated

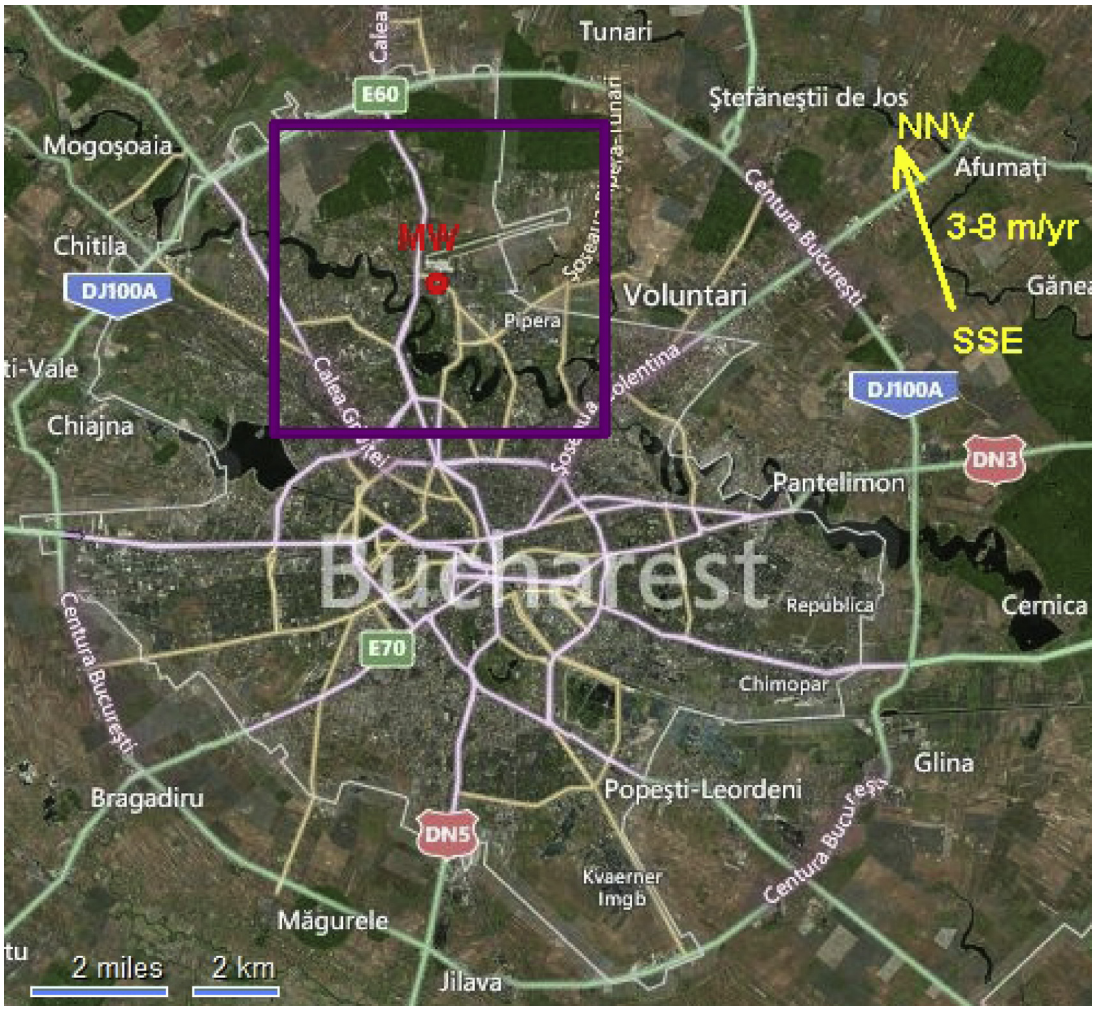

Fig. 1. The studied area (map retrieved after Bing-maps). The square represent the model discretization having in the middle a mono-well (MW) ATES system.

by a thermal insulation material. Several sections are perforated on the cold storage circuit (cold side filter). On top of those sections there is a shifting mechanism which redirects the pumped water from one circuit to the other. The next section is formed of a concrete casing which protects the submersible pump and the return pipe. Above there is another shifting mechanism, synchronized with the submerged one. The shifting mechanisms typically operate only twice a year, for the change of seasons.

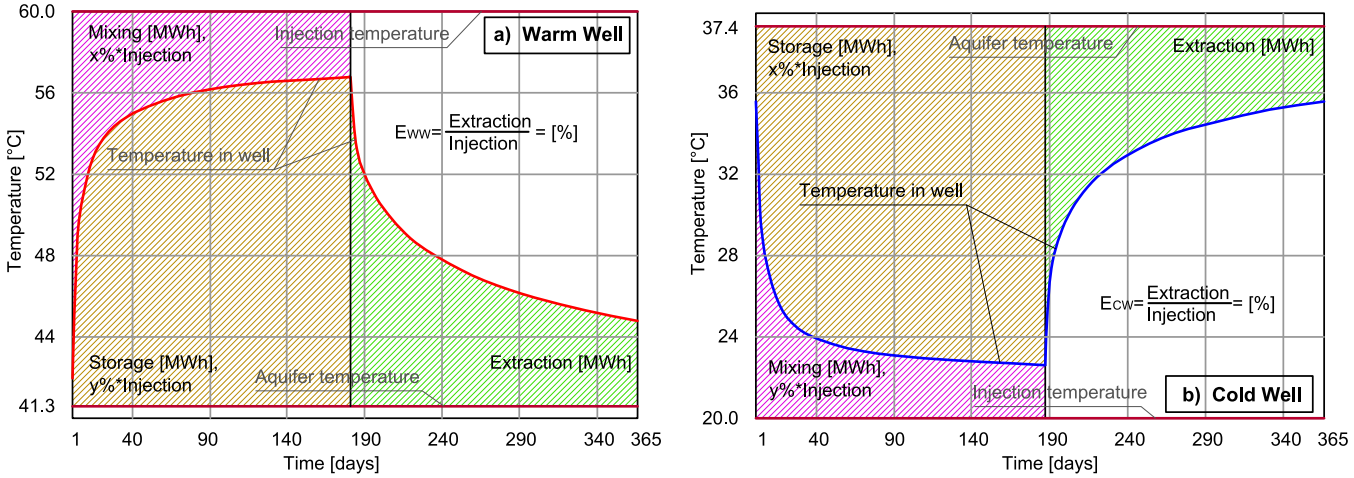

Fig. 2. Example of temperature profiles in wells for a HT-ATES system during the first year of operation.

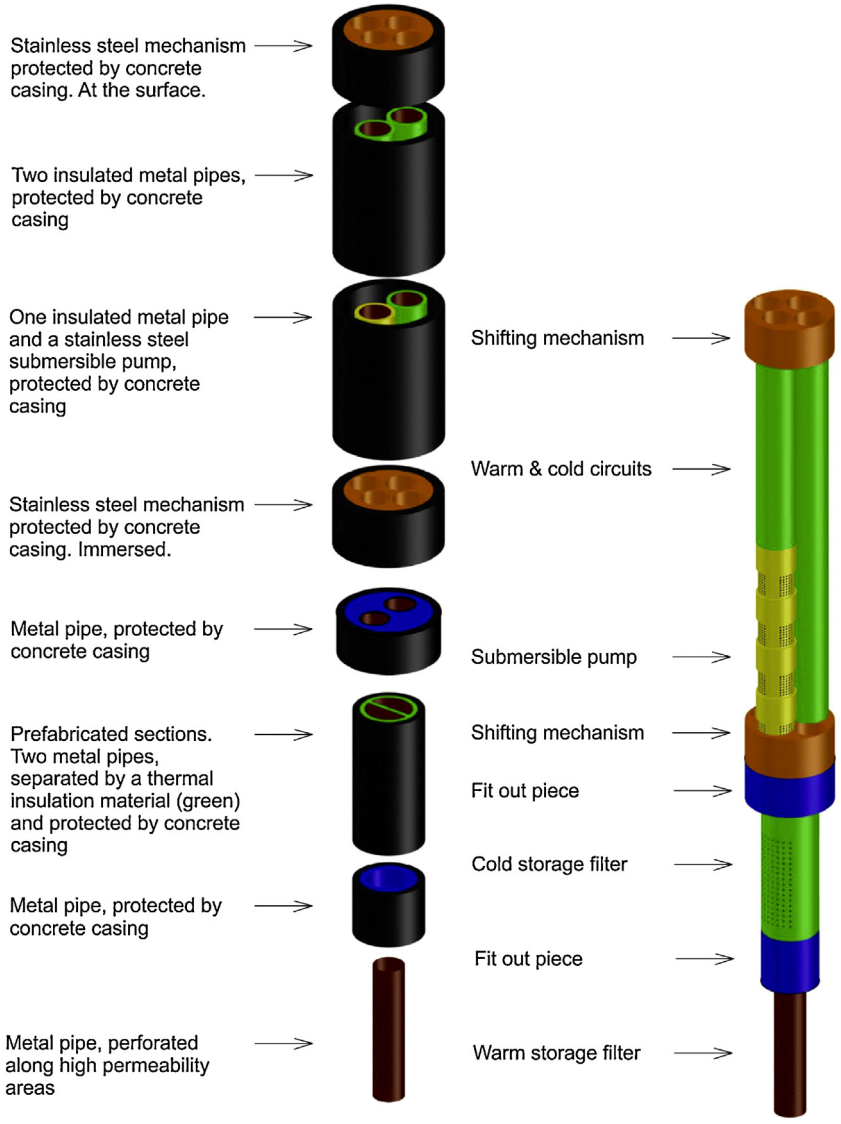

Fig. 3. 3D impression of a mono-well.

Table 1
Modelling parameters of the reference case.

Parameter	Symbol	Value	Units
Model particularities/properties			
Discretization (boundaries)	$L \times l$	8000×8000	m
Cells dimension in area of interest	$L \times l \times h$	$16 \times 16 \times 32$	m
Screen (filter) length	H	100	m
Flow rate	Q	10,500	m^3/day
Thermal radius of the storage	R_{th}	160	m
Injected water radius	R_w	190	m
Periods	P	21	–
Time frame	TF	10	years
Aquifer properties			
Horizontal hydraulic conductivity	K_h	60	m/day
Vertical hydraulic conductivity	K_v	30	m/day
Effective porosity	η	0.23	–
Brackish water density at 43 °C	ρ_0	991.8	kg/m^3
Brackish water viscosity at 43 °C	μ_0	1043	cp
Matrix density (bulk)	ρ_m	2300	kg/m^3
Longitudinal dispersivity	α_L	15	m
Transverse dispersivity	α_T	1.5	m
Bulk density	ρ_b	2200	kg/m^3
Thermal distribution coefficient	kd	0.00015	[m^3/kg]
Thermal diffusion coefficient	k	7.01E−10	m^2/s

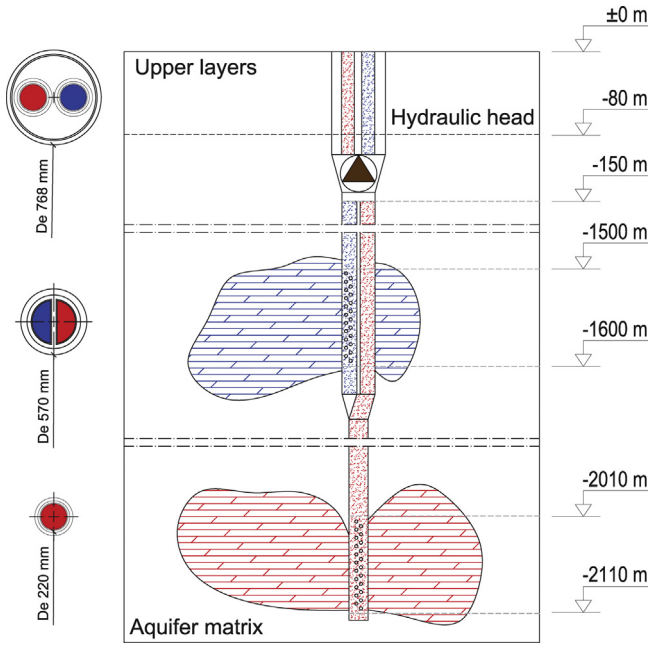

Fig. 4. Mono-well principle for the Bucharest case. Cold water filter is placed between −1500 m and −1600 m and the warm water filter is placed between −2010 m and −2110 m. Water is extracted from −150 m below surface by submersible pumping.

4. Methods used

To determine the performance of the mono-well ATES a numerical model was constructed. The temperature dependence of density and viscosity in the heat transport calculations were included by using SEAWAT (Langevin et al., 2008). To evaluate the significance of variable density and viscosity the simulations were also performed without this temperature dependence using MODFLOW 2000 (Halford and Hanson, 2002) and MT3DMS (Zheng, 2010). The rest of the simulations were performed only with SEAWAT.

4.1. Modelling procedure

The equation of state for fluid density was modified to vary with the temperature T of the fluid as well as the concentration C of a solute (Thorne et al., 2006) and it is written as:

$$\rho(C,T) = \rho_0 + \frac{\partial\rho}{\partial C}(C - C_0) + \frac{\partial\rho}{\partial T}(T - T_0) \quad (5)$$

where ρ_0 is the density of the undisturbed water used as reference density (Table 1), $\partial\rho/\partial C$ and $\partial\rho/\partial T$ represents the change in density with respect to concentration and temperature and C_0 and T_0 are prescribed initial concentration and temperature, assumed constant over time. The effect of viscosity variations on the resistance to ground water flow also was added through implementation of the relationship between permeability, viscosity, and hydraulic conductivity. Viscosity is incorporated into the flow equation as a function of both temperature and solute concentration.

In SEAWAT, the dynamic viscosity μ is implemented as temperature and/or concentration dependent in conductance equation. Written as:

$$COND = \frac{\mu_0}{\mu}\frac{T_r \cdot W}{L} = \frac{\mu_0}{\mu}\frac{K \cdot W \cdot H}{L} \quad (6)$$

where the conductance is expressed in terms of transmissivity T_r or hydraulic conductivity K, where W is the width of the cell, L is length of the cell and H represent the height of the cell. In the MODFLOW equation, Darcy's law is rewritten as $Q = COND(h_A - h_B)$, and runs together with SEAWAT(Langevin et al., 2008). $h_A - h_B$ is the head differences across the prism parallel to flow.

The dynamic viscosity variation is expressed as μ_0/μ where μ_0 is the initial dynamic viscosity of the aquifer (Table 1) and $\mu = \mu(C,T)$ calculated as:

$$\mu = \mu_0 + \sum_{k=1}^{NS}\frac{\partial\mu}{\partial C^k}(C^k - C_0^k) + \frac{\partial\mu}{\partial T}(T - T_0) \quad (7)$$

Table 2
Scenarios.

Parameter	Symbol	Units
Buoyancy	SEAWAT V.S. MT3D	–
Longitudinal dispersivity	10, 15, 20, 25, 30, 40, 50	metres
Flow variation	4500, 5700, 6900, 8100, 9300, 10,500	m^3/day
Vertical distance between filters	96, 160, 224, 288, 352, 410	metres
Multisystem interference	0.2, 0.5, 1, 2, 3	R_{th}

4.2. Parameters

Transient simulations were made; each for 10 calendar years. One calendar year is divided in 180 days of heating and 185 days of cooling, defined as periods. Each simulation starts with the background conditions of steady state regional flow in the NNW direction (1st period). The following 20 periods represent the summer (extracting from the cold storage) and winter seasons. The simulation ends with the winter season (extracting from the warm storage) in the 10th year.

The reference model (with values in Table 1) was used for all scenarios presented in this paper. In each scenario, one of the following parameters was varied with respect to the reference model: longitudinal dispersivity, mass flow rate, vertical distance between filters, and horizontal distance between multiple identical mono-wells. The scenarios are summarized in Table 2. The results were plotted in parallel for the warm and cold storage.

5. Results and discussion

The sensitivity of HT-ATES efficiency to the various parameters tested was analyzed to identify the best suitable conditions for HT-ATES exploitation. Several scenarios were built and compared with the reference case. Since the hot and cold storages in the HT-ATES system are not confined, the system behaviour was expected to differ from conventional ATES studies that focus on storage between confining layers.

5.1. Variable density effect

Results show that the efficiency obtained (Fig. 5) when considering density and viscosity variations in SEAWAT is significantly higher (>70% in the 10th year) than the efficiency obtained with the MT3D model (<67% in the 10th year). Whereas the efficiency for the warm and cold storage are similar for the MT3D case, efficiency increase for the SEAWAT model is higher for the warm well. The relatively lower efficiency increase for the cold well is explained by forced downward convection, in the direction of free convection that occurs due to the confining layer on top of the cold storage. Overall, density and viscosity variations therefore have a significant influence on the ATES performance in our case, as was observed by Grane and Gardner (1961).

The difference between SEAWAT and MT3D modelling is illustrated by the vertical cross section through the mono-well, for six time periods (Fig. 6). The temperature difference (SEAWAT – MT3D) was plotted on a scale between −2 ΔT and 2 ΔT. We observe a

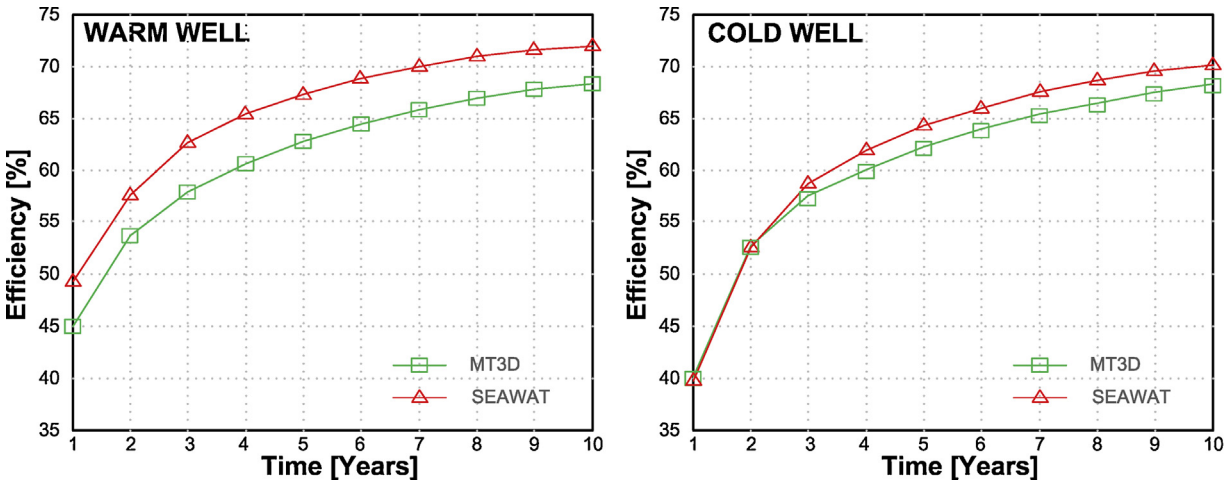

Fig. 5. Influence of variable density and viscosity on system efficiency. SEAWAT code uses variable density and viscosity with respect to temperature and MT3D uses constant density and viscosity.

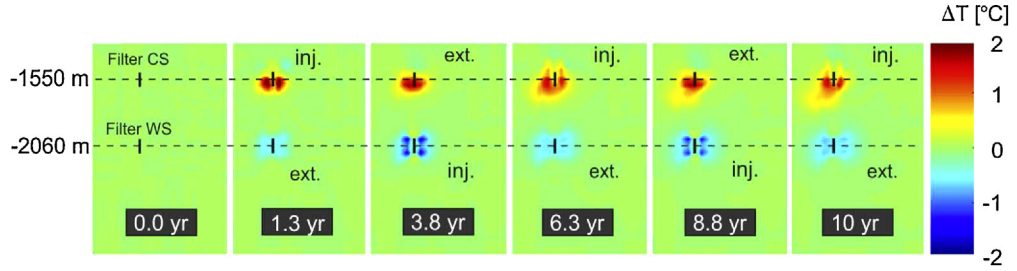

Fig. 6. Vertical cross section showing the temperature difference between SEAWAT modelling and MT3D modelling.

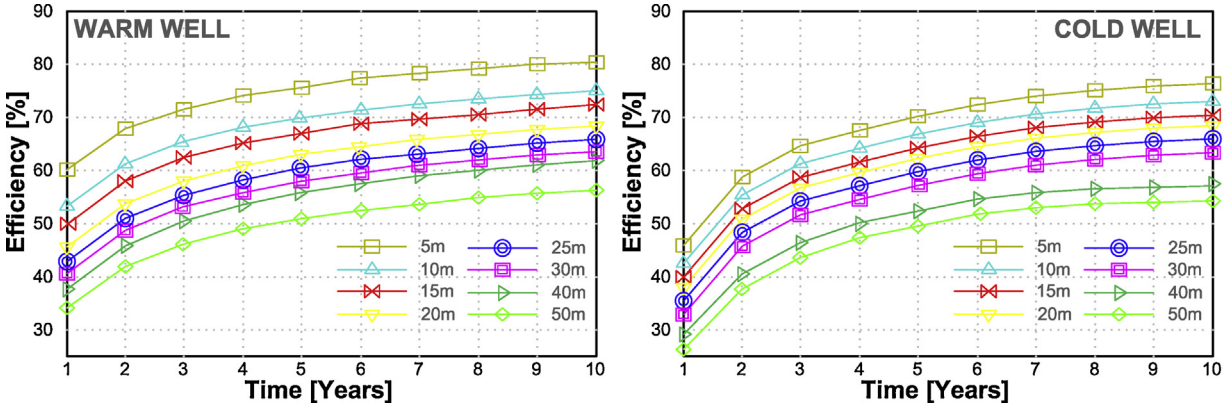

Fig. 7. Influence of longitudinal dispersivity on system efficiency. The ploted lines show the efficiency variation for different longitudinal dispersivity values (in metres).

positive anomaly below the cold filter, meaning the temperature at this location is higher for the case of non-density dependent flow. This is reasonable, since the cold storage in case of density dependent flow has the tendency to migrate downwards. Due to the significant discrepancies observed when neglecting density and viscosity differences, SEAWAT modelling was used for all other scenarios.

In the ATES well and the immediate surroundings, forced convection is dominant, powered by constant extractions/injections. In our case, based on the Richardson number (Ri = 2.2E−03), free convections is negligible Ri < 0.1 (Turner, 1973). In the vicinity (outside boundaries) of the thermal plumes, the Richardson number indicates a free convective flow (Ri = 3.46E+05). Here the buoyancy effect becomes significant but has less effect on the overall ATES efficiency.

5.2. Longitudinal dispersivity analyses

To test the model sensitivity regarding aquifer uncertainties, seven longitudinal dispersivity values were considered with the SEAWAT model. We set these values in accordance with similar studies to: 10 m (Bouw and Oude Essink, 2003; Yechieli et al., 2010; Terry and Chui, 2012), 30 m (Eusuff and Lansey, 2004); 50 m (Michael et al., 2013); 70–80 m (Ghassemi

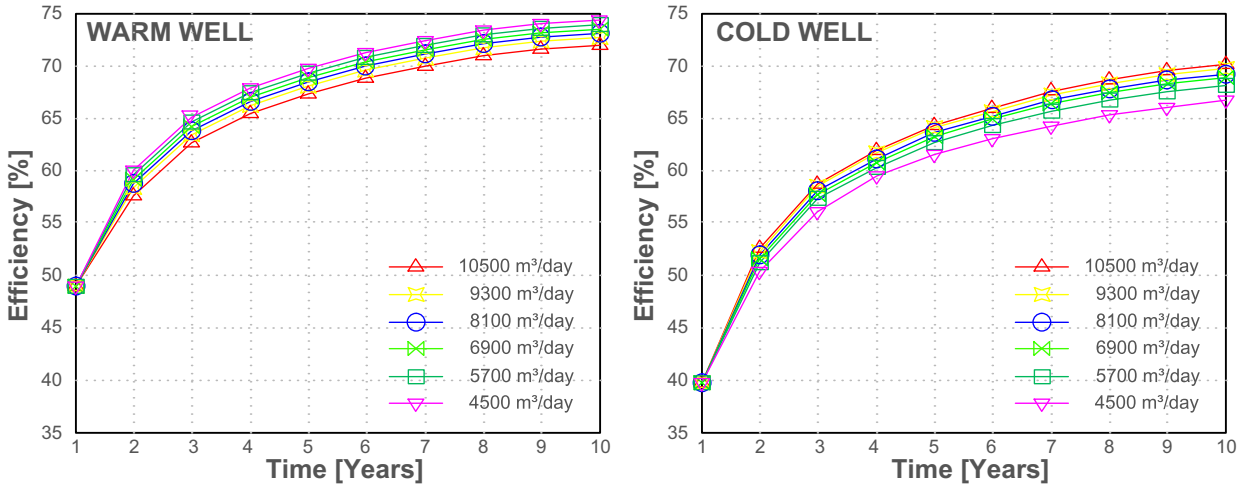

Fig. 8. Influence of pumping rates on system efficiency.

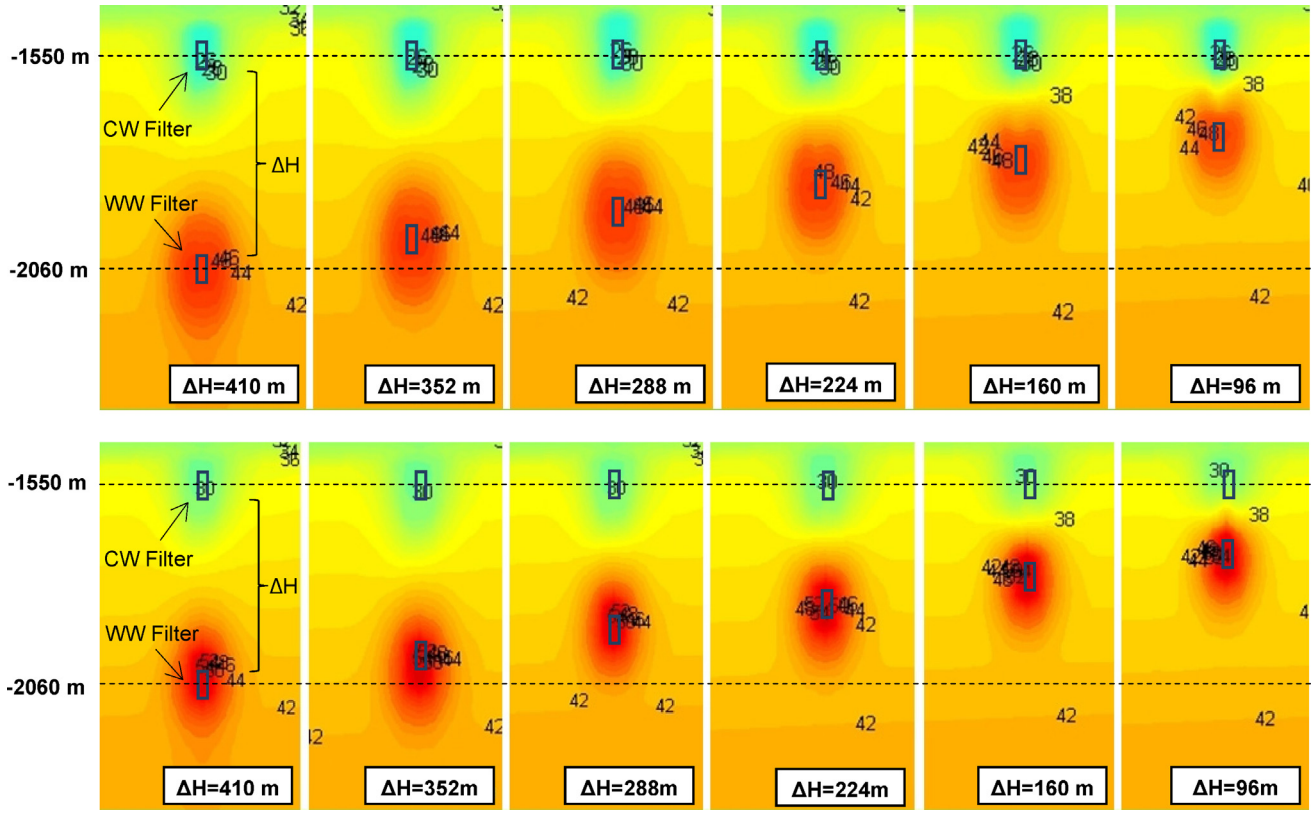

Fig. 9. Vertical cross sections showing the well filters. The warm storage filter was moved from 410 m (reference case) to 96 m. The pictures are coupled for the same ΔH having above the 10th year of operation, in the winter period (extraction from the warm well and injection in the cold well) and below the summer period (reversed process).

et al., 1990); 80–100 m (Kaleris, 2006) and100 m (Cobaner et al., 2012).

The results show that dispersivity has an important role in mixing and therefore affects the efficiency (Fig. 7). Therefore, we considered a longitudinal dispersivity of 15 m (red line in Fig. 7), with respect to the diagrams provided by Gelhar et al. (1992), based on the aquifer nature (limestone and dolomite) and the application scale (160 m). Horizontal transverse dispersivity was set as $\alpha_L \times 10^{-1}$ [m] and vertical transverse dispersivity as $\alpha_L \times 10^{-2}$ [m]. Thermal diffusion coefficient was set at 3.83×10^{-1} [m^2/s] for all simulations.

5.3. Workload variation

The objective of this analysis is to determine the system efficiency for reducing working loads down to 4500 [m^3/day] with respect to the workload in the reference scenario of 10,500 [m^3/day]. Strikingly, flow rate variation resulted in opposing impacts on system efficiency for the cold and warm storage (Fig. 8). Whereas in the warm storage, the efficiency increases with decreasing workloads, for the cold storage the efficiency decreases with decreasing workloads.

The behaviour of the cold storage is expected, as illustrated in Eq. (2), as the mixed convection ratio depends on the flow rate.

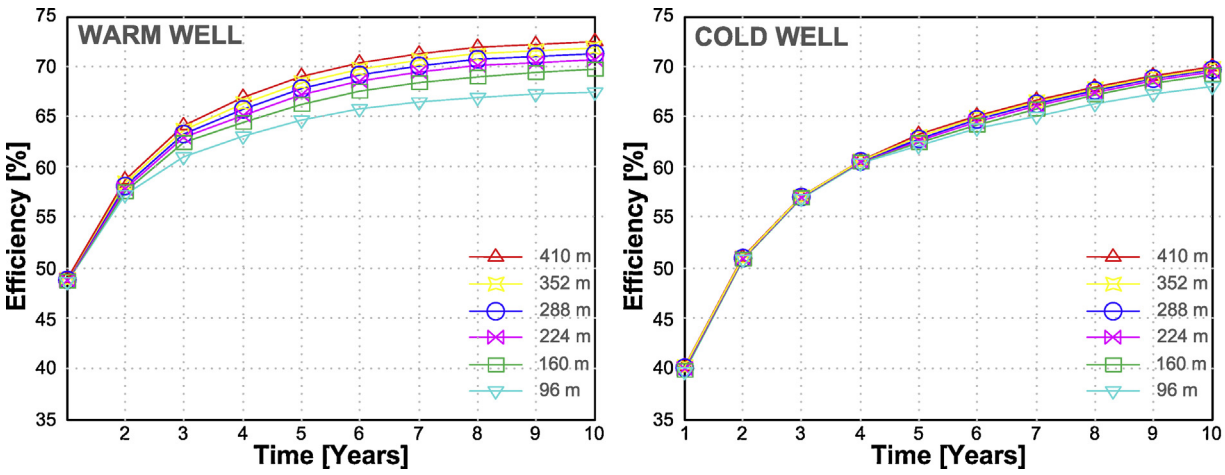

Fig. 10. Efficiency sensitivity for different filter positions (different distance between cold filter and warm filter).

Although, the cold storage is only confined by a cap rock aquitard at the top, this behaviour is typical though less pronounced as for fully confined ATES systems. For the warm storage however, the decreasing efficiencies with increasing working loads are explained by the combination of lower viscosities at higher temperature and the increased upward pressure gradient in the absence of a confining layer between the hot and cold storage.

Decreasing the workload, results in proportionally twice the decrease in the upward oriented pressure gradients. The workload is being extracted from the overlying cold storage as it is being injected in the underlying warm storage. As the hydraulic conductivity K is inversely proportional with viscosity, the decreasing viscosities at higher temperatures of the warm storage will enhance the vertical permeability of both free and forced upward convection components. The decreasing efficiency by loss of warm water with increasing workloads is therefore directly proportionally to the extent to which the forced flow component in the vertical direction, acts in the upward direction of free flow in the warm storage. In contrast, for the cold storage, the enhancement of the downward oriented free flow component is limited by the reduced viscosity at lower temperatures, contributing to a net increase of efficiency with increasing workloads. Hence, higher working load will act to reduce the contrast between warm and cold storage efficiencies.

5.4. Variations of the vertical distance between injection/extraction filters (ΔH)

The effect of decreasing the vertical separation of the warm storage with respect to the cold storage is illustrated with vertical cross sections for the 10th operational year (Fig. 9). The distance between cold and warm filters (ΔH) was decreased from 410 m in the reference case down to 96 m. The simulation with a ΔH of 96 m showed a significant decrease of efficiency for both storages as shown in Fig. 10. For the warm storage, as with the effect of increased workloads, the decreased distance resulted in increased upward pressure gradients in the direction of free convection. In addition, the efficiency decrease was larger for the warm well as it was affected by the lower environmental temperatures at shallower depths, as the warm filter was moved upward towards the cold filter.

5.5. Mono-well ATES multi-system interferences

To test the ability to further increase heat and cold storage capacity, the optimal distance between wells for five identical mono-well ATES systems was considered (MW1, MW2, MW3, MW4, MW5), operating with identical injection temperatures (20 °C and 60 °C) and flow rates (10,500 m^3/day). The distances were set as multiples of the thermal radius, starting from $0.2 \times R_{th}$ up to $3.0 \times R_{th}$ (Fig. 11).

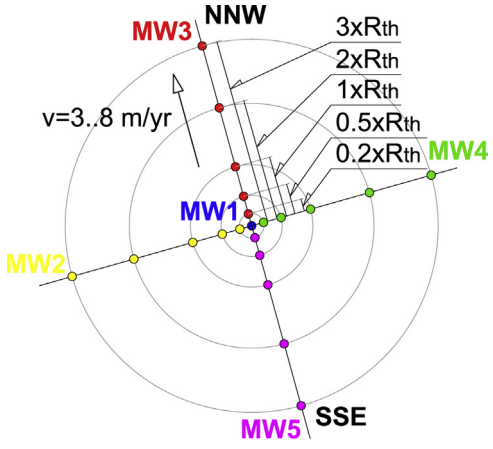

Fig. 11. Mono-well multisystem setup. Five simulations were made by displacing the mono-wells symmetrically, with respect to the regional flow direction and the reference system (MW1). In the first simulation all wells were placed at 0.2 R_{th} from each other (32 m). Regional flow direction is indicated by the black arrow on NNW. The velocity is estimated between 3 and 8 m per year, depending on location and depth.

For the individual well performances, as shown in Fig. 12, smaller well separation distances lead to higher energy efficiencies, as compared to individual systems (e.g. Fig. 5). This is reasonable, because for small well-to-well distances, the five wells form a single thermal plume (cluster) which gives a lower area to volume ratio than for five separate plumes, resulting in lower energy loss at the boundaries of the plume. MW1 has the highest efficiency, as its central position in between other wells, limits heat losses by interaction with the surrounding lower environmental temperature. Individual well performances of the outer wells, is highest for MPW3 and lowest for MPW5. As these wells are respectively located at the down-gradient and up-gradient side of the of regional groundwater flow direction, heat lost from up-gradient systems is captured by MW3.

By increasing the well separation distance the systems efficiencies decreases, and for clusters with $1 \times R_{th}$. For $2 \times R_{th}$ and $3 \times R_{th}$ well separation distances, the efficiencies of the individual wells are similar as for the reference case for a single HT-ATES system (Fig. 5). Therefore, for district heating and cooling applications, where more

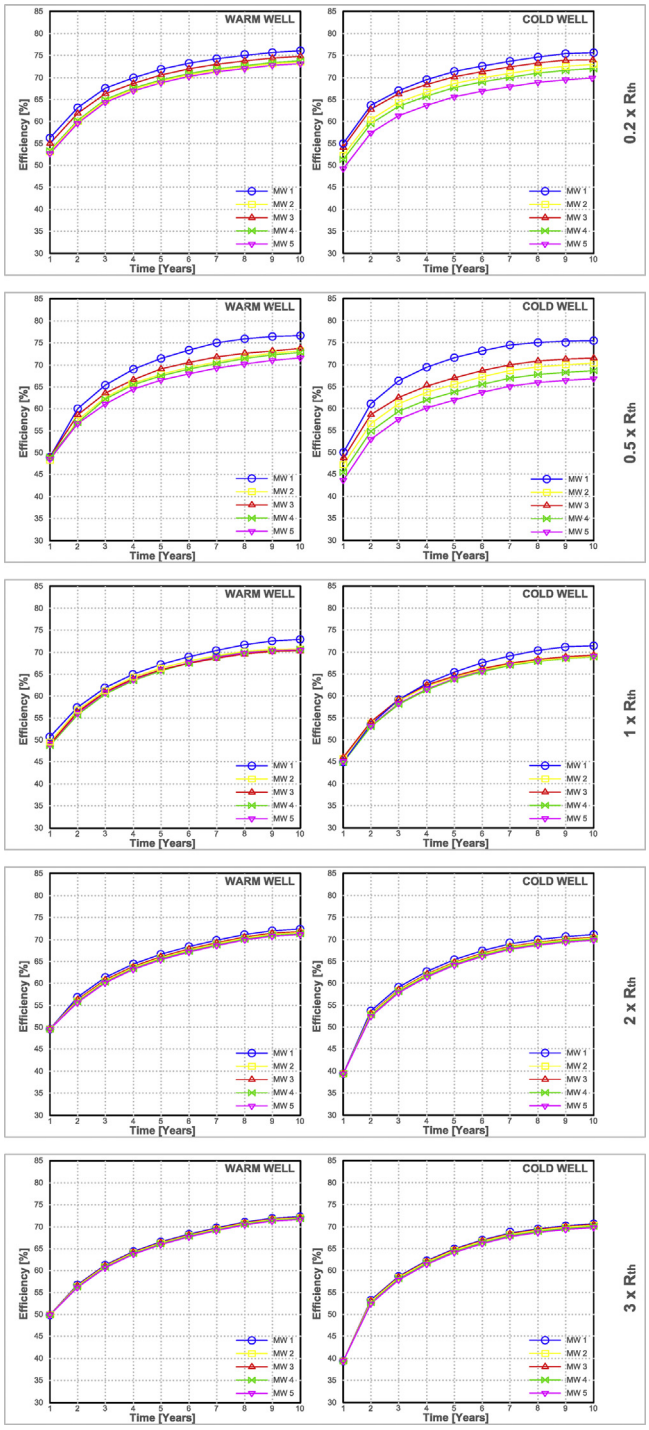

Fig. 12. Multi-system interferences. This picture shows the efficiency sensitivity for five identical mono-well HT-ATES systems with respect to the length between them and the regional flow.

than one mono-well system is necessary, the smallest well separation distance ($0.2 \times R_{th}$ in our case) gives the best overall efficiency for the cluster of wells.

6. Conclusions

Our study has demonstrated the potential of using HT-ATES mono-well systems, even in the absence of suitable confining layers for separation of the hot and cold storage volumes. In addition, we have explored a range of conditions for which this is possible and the sensitivity of the thermal efficiency of the ATES system for various parameters.

Numerical modelling was used to determine the performance of a planned HT-ATES system with a mono-well. For the reference case, our simulations show that the energy efficiency of a single HT-ATES mono-well system increases from around 40% initially to 70% over the first 10 years of operation. The influence of several physical and design parameters on the overall efficiency was evaluated. Especially aquifer heterogeneity, represented by the thermal dispersivity, was found to have a large influence on the resulting energy efficiency. Due to increasing thermal losses caused by dispersion, the energy efficiency after 10 years ranges from 80% to 55% for dispersivities of 5 to 50 m, respectively. This emphasizes the need for careful aquifer selection and characterization for HT-ATES projects to be successful.

Also, consideration of variable density and viscosity in the use of SEAWAT for the numerical simulations was required to accurately describe HT-ATES behaviour. This consideration resulted in significantly higher estimated efficiencies than for the scenarios that assumed density and viscosity independent of temperature.

Since the amount of groundwater that is extracted and injected within ATES systems is typically determined by the end-user demand, we have investigated the sensitivity of the energy efficiency for different groundwater flow regimes. With workloads increasing from 4500 to 10,500 m^3/day, the cold storage efficiency improved from 67.5% to 70.2% while the warm storage efficiency declined from 74.3% to 72.5%, due to the lowered viscosity that enhanced free convection.

The warm and cold storage of ATES doublet systems are typically placed at similar depths at some lateral distance. We showed that when aquifer thickness is sufficient, cold storage can also be placed above the warm storage, saving on drilling costs. However, for such a mono-well ATES system numerical simulations are required to ensure sufficient vertical separation. The minimal distance to avoid interference for the tested conditions in this study was 160 m.

Finally, the thermal interference between multiple HT-ATES mono-well systems was evaluated by considering a group of 5 identical mono-wells. Our simulations show that the thermal efficiency of a well is not improved when the distance to the other wells is larger than $2 \times R_{th}$. However, when this distance is reduced to $0.2 \times R_{th}$, the overall energy efficiency is increasing with 5%, relative to $3 \times R_{th}$ scenario. This shows that grouping multiple mono-well ATES systems in areas with large energy demand enables higher energy efficiencies due to positive thermal interference.

Acknowledgements

We gratefully acknowledge the constructive comments and suggestions provided during the peer review process by the editor and by the anonymous reviewers.

References

Aydin, O., Kaya, A., 2009. MHD mixed convection of a viscous dissipating fluid about a permeable vertical flat plate. Appl. Math. Model., 4086–4096.
Anderson, M.P., 2005. Heat as a ground water tracer. GroundWater 43 (6), 951–968.
Bakr, M., van Oostrom, N., Sommer, W., 2013. Efficiency of and interference among multiple aquifer thermal energy storage systems; a Dutch case study. Renew. Energy, 53–62.
Bandrabur, T., Craciun, P., Giurgea, P., 1983. Geological and Hydro-geological Study of Moesian Platform (between Arges and Danube) to Explore the Thermal Aquifers Potential (in Romanian), Archive report IGG, Bucharest.
Bandrabur, T., 1988. Research, Evaluation and Exploitation of Geothermal Resources Potential of the Hydro-geothermal Basin in Bucharest-Otopeni (in Romanian), Archive report IGG, Bucharest.
Bear, J., 1972. Dynamics of Fluids in Porous Media., ISBN 0486656756.
Bonte, M., Van Breukelen, B., Stuyfzand, P., 2012. Environmental impacts of aquifer thermal energy storage investigated by field and laboratory experiments. In: World Congress on Water, Climate, Energy, Dublin.

Bouw, L., Oude Essink, G.H.P., 2003. Fluid flow in the northern Broad Fourteens basin during late Cretaceous inversion. NL J. Geosci., 55–69.
Carotenuto, A., Fucci, F., La Fianza, G., Reale, F., 1991. Physical model and demonstration of an aquifer thermal energy store. Heat Recovery Syst. CHP 11 (2–3), 169–180.
Chaudhuri, A., Sekhar, M., 2006. Stochastic modelling of solute transport in 3D heterogeneous porous media with random source condition. Stoch. Environ. Res. Risk Assess., 159–173.
Cobaner, M., Yurtal, R., Dogan, A., Motz, L.H., 2012. Three dimensional simulation of seawater intrusion in coastal aquifers: a case study in the Goksu Deltaic Plain. J. Hydrol., 262–280.
Doughty, C., Hellstrom, G., Tsang, C.F., 1982. A dimensionless parameter approach to the thermal behavior of an Aquifer Thermal Energy Storage. Water Resour. Res., 571–587.
Drijver, B., 2011. High Temperature Aquifer Thermal Energy Storage (HT-ATES): water treatment in practice. In: Nationaal Congres Bodemenergie Proceedings.
Drijver, B., Aarssen, M.V., Zwart, B., 2012. High-temperature Aquifer Thermal Energy Storage (ATES): Sustainable and Multi-usable. Paper presented at Innostock 2012.
Edworthy, K.J., Puri, S., 1986. Groundwater and aquifers; an overview of 'exotic' uses. Q. J. Eng. Geol. Hydrogeol., 87–95.
Eusuff, M.M., Lansey, K.E., 2004. Optimal operation of artificial groundwater recharge systems considering water quality transformations. Water Resour. Manage., 379–405.
Ferguson, G., 2007. Heterogeneity and thermal modelling of ground water. Ground Water, 485–490.
Fridleifsson, I.B., Bertani, R., Huenges, E., Lund, J.W., Ragnarsson, A., Rybach, L., 2008. The possible role and contribution of geothermal energy to the mitigation of climate change. In: Proceedings, Luebeck, Germany.
Gao, Q., Li, M., Yu, M., Spitler, J.D., Yan, Y.Y., 2009. Review of development from GSHP to UTES in China and other countries. Renew. Sust. Energy, 1383–1394.
Gelhar, L.W., Welty, C., Rehfeldt, K.R., 1992. A critical review of data on filed-scale dispersion in aquifers. Water Resour. Res., 1955–1974.
Ghassemi, F., Jakeman, A.J., Jacobson, G., 1990. Mathematical modelling of sea water intrusion, Nauru island. Hydrol. Process, 269–281.
Grane, F.E., Gardner, G.H.F., 1961. Measurements of transverse dispersion in granular media. J. Chem. Eng., 283–287.
Halford, K.J., Hanson, R.T., Santa Clara Valley Water District (Calif.), Geological Survey (U.S.), 2002. User Guide for the Drawdown-Limited, Multi-Node Well (MNW) Package for the U.S. Geological Survey's Modular Three-Dimensional Finite-Difference Ground-Water Flow Model, Versions MODFLOW-96 and MODFLOW-2000. U.S. Dep. of the Interior, U.S. Geol. Surv., Sacramento, CA.
Hassanizadeh, S.M., 1990. Experimental study of coupled flow and mass transport: a model validation exercise in calibration and reliability in groundwater modelling. In: Proceedings, IAHS, pp. 241–250.
Hassanizadeh, S.M., Leijnse, A., 1995. A non-linear theory of high-concentration gradient dispersion in porous media. Adv. Water Resour., 2003–2015.
Hopmans, J.W., Simunek, J., Bristow, K.L., 2002. Indirect estimation of soil thermal properties and water flux using heat probe measurements: geometry and dispersion effects. Water Resour. Res. 38 (1), 7–14.
Kabus, F., Wolfgramm, M., Seibt, A., Richlak, U., Beuster, H., 2009. Aquifer thermal energy storage in Neubrandenburg – monitoring throughout three years of regular operation. In: Proceedings, Effstock, Sweden.
Kaleris, V., 2006. Marine groundwater discharge: effects on hydrogeology and of near shore surface water bodies. J. Hydrol., 96–117.
Kim, J., Lee, Y., Yoon, W.S., Jeon, J.S., Koo, M.-H., Keehm, Y., 2010. Numerical modelling of aquifer thermal energy storage system. Energy, 4955–4965.
Langevin, C.D., Thorne, D.T., Dausman, A.M., Sukop, M.C., Guo, W., 2008. SEAWAT Version 4: A Computer Program for Simulation of Multi-species Solute and Heat Transport. U.S. Geological Survey Techniques and Methods, Book 6, Chapter A22.
Marsily, G., 1986. Quantitative Hydrogeology., ISBN 0-12-208915-4.
Michael, H.A., Russoniello, C.J., Byron, L.A., 2013. Global assessment of vulnerability to sea-level rise in topography-limited and recharge-limited coastal groundwater systems. Water Resour. Res., 2228–2240.
Molz, F.J., Warman, J.C., Jones, T.E., 1978. Aquifer storage of heated water: Part I – A field experiment. Ground Water, 234–241.
Molz, F.J., Parr, A.D., Andersen, P.F., Lucido, V.D., Warman, J.C., 1979. Thermal energy storage in a confined aquifer: experimental results. Water Resour. Res., 1509–1514.
Molz, F.J., Parr, A.D., Andersen, P.F., 1981. Thermal energy storage in a confined aquifer: second cycle. Water Resour. Res., 641–645.
Molz, F.J., Melville, J.G., Parr, A.D., King, D.A., Hopf, M.T., 1983. Aquifer thermal energy storage: a well doublet experiment at increased temperatures. Water Resour. Res., 149–160.
Nick, H.M., Schotting, R., Gutierrez-Neri, M., Johannsen, K., 2008. Modelling Transverse Dispersion and Variable Density Flow in Porous Media. Springer.
Yechieli, Y., Shalev, E., Wollman, S., Kiro, Y., Kafri, U., 2010. Response of the Mediterranean and Dead sea coastal aquifers to sea level variations. Water Resour. Res. 46.
Sanner, B., Karytsas, C., Mendrinos, D., Rybach, L., 2003. Current status of ground source heat pumps and underground thermal energy storage in Europe. Geothermics, 579–588.
Schotting, R.J., Moser, H., Hassanizadeh, S.M., 1999. High-concentration-gradient dispersion in porous media: experiments, analysis and approximations. Water Resour. Res., 665–680.
Smith, L., Chapman, D.S., 1983. On the thermal effects of groundwater flow 1. Regional scale systems. Geophys. Res., 593–608.
Sommer, W.T., Valstar, J., Gaans, P., Grotenhuis, T., Rijnaarts, H., 2013. The impact of aquifer heterogeneity on the performance of Aquifer Thermal Energy Storage. Water Resour. Res., 8128–8138.
Terry, J.P., Chui, T.F.M., 2012. Evaluation the fate of freshwater lenses on atoll islands after eustatic sea-level rise and cyclone-driven inundation: a modelling approach. Global Planet. Change, 76–84.
Thorne, D., Langevin, C.D., Sukop, M.C., 2006. Addition of simultaneous heat and solute transport and variable fluid viscosity to SEAWAT. Comput. Geosci. J., 1758–1768.
Tsang, C.F., Hopkins, D.L., Hellstrom, G., 1980. Aquifer Thermal Energy Storage: A Survey. Lawrence Berkeley National Laboratory, LBL-10441.
Turner, J.S., 1973. Buoyancy Effects in Fluids., ISBN 0-521-08623-X.
Vandenbohede, A., Lebbe, L., 2003. Combined interpretation of pumping and tracer tests: theoretical considerations and illustration with a field test. J. Hydrol., 134–149.
Vandenbohede, A., Lebbe, L., 2006. Double forced gradient tracer test: performance and interpretation of a field test using a new solute transport model. J. Hydrol., 155–170.
Vandenbohede, A., Louwyck, A., Lebbe, L., 2008. Identification and reliability of microbial aerobic respiration and denitrification kinetics using a single-well push–pull field test. J. Contam. Hydrol., 42–56.
Vandenbohede, A., Louwyck, A., Lebbe, L., 2009. Conservative Solute Versus Heat Transport in Porous Media During Push–pull Tests.
Ward, J.D., Simmons, C.T., Dillon, P.J., 2007. A theoretical analysis of mixed convection in aquifer storage and recovery: how important are density effects? J. Hydrol., 169–186.
Zeghici, R., Damian, A., Frunzulică, R., Iordache, F., 2014. Energy performance assessment of a complex district heating system which uses gas-driven combined heat and power, heat pumps and high temperature aquifer thermal energy storage. Energy Build., 142–151.
Zeghici, R.M., Hartog, N., Sommer, W., 2013. Aquifer thermal energy storage: cold storage process in a geothermal ATES. In: AquaConSoil ThS, p. A3.
Zheng, C., 2010. MT3DMS v5.3 A Modular Three-Dimensional Multispecies Transport Model for Simulation of Advection, Dispersion and Chemical Reactions of Contaminants in Groundwater Systems: Supplemental User's Guide. Univ. of Ala., Tuscaloosa.
Zuurbier, K.G., Hartog, N., Valstar, J., Post, V.E.A., van Breukelen, B.M., 2013. The impact of low-temperature seasonal aquifer thermal energy storage (SATES) systems on chlorinated solvent contaminated groundwater: modelling of spreading and degradation. J. Contam. Hydrol., 1–13.